Shock and Vibration 20 (2013) 561–573
DOI 10.3233/SAV-130768
IOS Press

Development of time-reversal method for impact source identification on plate structures

Chunlin Chen[a,b], Yulong Li[a] and Fuh-Gwo Yuan[b,*]
[a]*School of Aeronautics, Northwestern Polytechnical University, Xi'an, Shaanxi, China*
[b]*Department of Mechanical and Aerospace Engineering, North Carolina State University, Raleigh, NC, USA*

Received 1 January 2012
Revised 28 February 2012
Accepted 4 March 2012

Abstract. This paper presents a detailed study on the impact source identification of a plate structure using time-reversal (T-R) method. Prior to impact monitoring, the plate is calibrated (or characterized) by transfer functions at discrete locations on the plate surface. Both impact location and impact loading time-history are identified using T-R technique and associated signal processing algorithms. Numerical verification for finite-size isotropic plates under low velocity impacts is performed to demonstrate the versatility of T-R method for impact source identification. The tradeoff between accuracy of the impact location detection and calibration spacing is studied in detail. In particular, the effect of plate thickness on calibration spacing has been examined. A number of parameters selected for determining the impact location, approximated transfer functions and steps taken for reconstructing the impact loading time-history are also examined. Two types of noise with various intensities contaminated in strain response and/or transfer functions are investigated for demonstrating the stability and reliability of the T-R method. The results show that T-R method is robust against noise in impact location detection and force reconstruction in circumventing the inherent ill-conditioned inverse problem. Only transfer functions are needed to be calibrated and four sensors are requested in T-R method for impact identification.

Keywords: Impact location detection, impact force reconstruction, time-reversal method, calibration spacing, noise effect

1. Introduction

The safety and reliability of aerospace structures are always alerted by various external impact sources, including tool drops, runway debris, hails, birds and unknown events. Especially for composite structures, the mechanical stiffness and strength can be degraded significantly by the barely visible impact damage (BVID) [1]. However, the conventional nondestructive evaluation (NDE) techniques [2], such as radiographic testing, ultrasonic testing, eddy current, and infrared thermography technique, are time consuming and labor intensive because in many cases partial disassembly is required in order to assess critical locations. Impact monitoring techniques have been developed to detect the impact location and reconstruct the impact loading time-history on structures while in service using a permanently mounted array of sensors. With the identified impact source, the associated damages caused by the impact and its residual strength can be conducted by on-ground testing databases.

*Corresponding author: Fuh-Gwo Yuan, Department of Mechanical and Aerospace Engineering, North Carolina State University, Raleigh, NC 27695, USA. Tel.: +1 919 515 5947; Fax: +1 919 515 7968; E-mail: yuan@ncsu.edu.

ISSN 1070-9622/13/$27.50

The identification of impact source based on sensor data and some characteristics of the structure is an inverse problem. Mathematically, the inverse problem is often both *nonlinear* and *ill-posed* [3,4]. By ill-posedness, it means that one of the following conditions is violated: the existence of the solution; the uniqueness of the solution; or the continuous dependence of the solution on the data (stability condition). In impact source identification problems, the uniqueness and the stability of the solution are generally violated because of incomplete information collected by a practically limited number of sensors, the existence of measurement error and noise, and etc. Thus, the stability and reliability of the impact identification method are at least as important as its accuracy.

The objective of the impact source identification is to determine the impact location and impact loading time-history. In order to avoid possible non-unique solutions, impact location is usually detected first followed by impact loading time-history reconstruction. The time difference of arrival (TDOA) of sensor signals received by spatially distributed sensors is commonly utilized to localize the source in many application areas [5]. Based on the time of first-arrival of a particular wave mode and its velocity information, the triangulation method has been widely used to estimate the impact location of different types of plate [6–8]. However the accurate time-of-flight and wave velocity information are often difficult to be obtained in practice, especially for noisy signals, the complex structures with joints and stiffeners, and the wave velocity is directionally dependent in composites. Recently several attempts have been made using wavelet transformation and wavelet decomposition to get the accurate arriving time [9,10]. Kundu and coworkers [11] improved the triangulation method for an anisotropic plate by minimizing objective functions. An optimization method has been proposed to estimate the impact location by the predicted forces at all candidate impact locations [12]. The estimated impact location is chosen from the calibration points and the computation may be very complex for large structures. Park and Chang [13,14] detected the impact location by mapping the power distribution over the entire structure using the uniformly distributed sensors, thus many sensors required. The authors [15] further improved this method by optimizing the number and the locations of sensor based on a genetic algorithm. Artificial Neural network (ANN) [16] has been used to solve this class of the problem for its versatility, but it requires a large amount of training data. Tracing the impact location with a few sensors accurately and rapidly remains one of the challenges in impact monitoring.

It is impractical to measure the impact loading history directly in impact monitoring. The impact force is often computed by the impact response signals received from sensors and the characteristic information of the structures, such as Green's function or transfer function, which is the physical relationship between the impact force and its response. Finite element method [12] and analytical solution by plate theory [17,18] could be used to obtain these functions conveniently; however, these methods are only suitable for infinite plate or simple structure because the material properties and boundary condition of the complex structures may not be known precisely in practice. Transfer functions can be calibrated directly by experiments [19,20] for all structures, but the argument between the accuracy and the time consumption should be considered. Based on these functions in time or frequency domain, a deconvolution technique is commonly used to solve this inverse problem. An Auto-Regressive with eXogenous input (ARX) model has been applied to reconstruct the loading history [16,21]. In fact, the ill-conditioned nature of the inverse problem had not been overcome by deconvolution technique or the ARX model. Normally the ill-conditioning nature of reconstructing the impact loading time-history is remedied by using regularization techniques to handle the ill-posedness of inverse problems [20]. Impact force could be reconstructed by ANN [22] method without transfer functions. However, the training process may be too complex to be practical for the training data should be generated in any type of loading history at all locations. The feasibility and stability of the method for force reconstruction are the key outstanding issues in applications.

The T-R method [23–27] has been widely used in many diverse disciplines such as seismology, biomedical imaging, acoustics, and structural health monitoring for its capability to unravel the excitation source in various media. Figure 1 illustrates the two operation steps of the T-R procedure [23]. In the recording step (left), the distorted pressure field from a point like source is measured on the cavity elements; in the reconstruction step (right), the recorded signals are time-reversed and remitted by the sensors. The time-reversed pressure field back-propagates and refocuses exactly on the initial source. Xu and Giurgiutiu [28] studied the Lamb wave T-R method with piezoelectric wafer active sensors for damage detection. The applicability of a T-R method in modern acoustics to health monitoring of a composite plate is investigated by Park et al. [29]. Ciampa and Meo [30] developed a one channel T-R imaging method to detect the impact location in reverberant complex composite structures. Combining the T-R focusing concept and a complex Shannon wavelet transform algorithm, the impact monitoring of an aircraft wing box has been demonstrated by Qiu et al. [31].

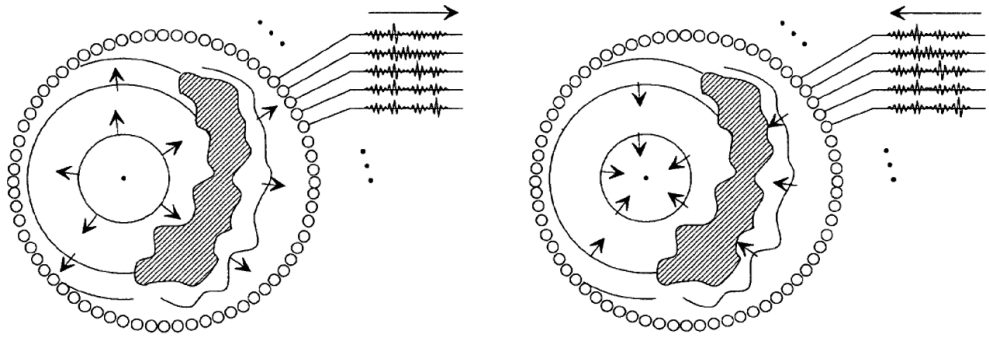

Fig. 1. Two operation steps of time-reversal procedure [23].

An impact source identification method based on T-R method was developed by the authors [32]. The impact location was roughly estimated by choosing the maximum peak amplitude of reconstructed signals among a few selected calibration locations. Then a finer location search algorithm based on a local optimal search scheme was proposed to determine the impact location at nearby area. Some parameters in T-R method, such as time duration of T-R process, number and spatial distribution of sensors, reconstruction of force with various shapes and frequency have been discussed in the author's previous work [32]. However, a key issue regarding the practicality of the T-R method, the spacing of the transfer functions is needed to be studied in detail before this impact source identification method is validated experimentally. For example, it is impractical to calibrate the transfer function on a plate structure with 10 mm spacing in a 420 mm×420 mm×1 mm plate, requiring over 1,800 calibration tests. Thus, the feasibility, stability and reliability of T-R method for impact identification are required for further study. The spacing of the calibration location of transfer functions for plates with various thicknesses, the selection of characteristic parameters in location detection, transfer function approximation, the effect of noise in impact location detection and force reconstruction by approximated transfer functions are to be investigated in detail as follows.

2. The method for impact source identification

To verify the robustness of the T-R method to identify the impact source, a finite element method (FEM) is employed to generate synthetic data. It is worth of noting that the FEM is merely used to generate data to validate the T-R method, the synthetic data can be readily replaced by sensor data in practice. It aims at investigating the characteristic of time reversal method for impact source identification. An aluminum plate is of dimension 420 mm×420 mm×1 mm and the four sensors are mounted near the corner of the plate by 40 mm from each side. The plate is simply supported on all edges. The mechanical properties of the aluminum are $E = 72$ GPa, $\nu = 0.3$, $\rho = 2700$ Kg/m^3. To investigate the effect of plate thickness on the selection of calibration location spacing and impact location detection, thicknesses ranging from 1 mm to 4 mm are studied. Figure 2 shows the locations marked on the plate when the calibration spacing is 20 mm, which will be discussed later.

2.1. The time-reversal procedure

For impact events where the dimension of the impact object is smaller than the smallest wavelength of the waves propagating in the plate, the impact source can be treated as a point source. The transfer function (Green's) represents the relationship between the calibrated impact force acting at the location, ξ, in the plate and the strain response observed at a sensor location are calibrated in frequency domain by

$$G_i(\xi, \omega) = \frac{S_i(\omega)}{F(\xi, \omega)} \tag{1}$$

where $F(\xi,\omega)$ is calibration force at the location ξ, $S_i(\omega)$ is the summation of the in-plane strain response $(\varepsilon_x + \varepsilon_y)$ proportional to the output voltage measured by the i^{th} piezoelectric sensor.

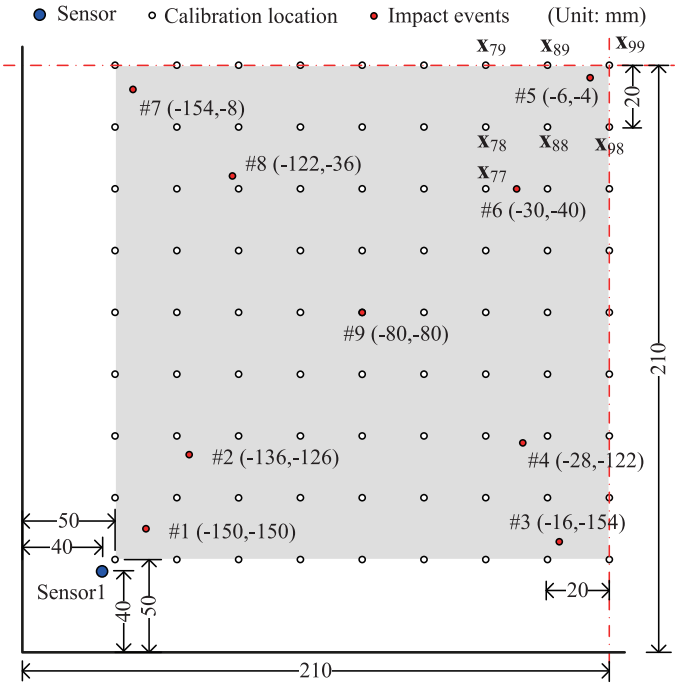

Fig. 2. Sensor, impact location and calibration locations with 20 mm spacing.

The T-R procedure for impact source identification is based on transfer functions. First the plate is calibrated by discrete calibration points (locations), usually evenly spaced within the enclosed sensor area. Issues related to the calibration location spacing on impact location detection and reconstructing the impact source characteristics will be discussed in next few sections. In this simulation, the forces used to calibrate the plate are a half-sinusoidal wave with time duration of 100 μs. It covers the frequency range of most practical impact forces with time duration 0.1–10 ms.

Mathematically the T-R procedure can be realized through transfer functions. Transfer functions between any two arbitrary points in the plate are reciprocal based on its spatial reciprocity. The in-plane strains measured by all the sensors are used to reconstruct the impact source characteristics. Based on transfer functions derived from Eq. (1), the T-R procedure in frequency domain can be expressed by

$$f_i(\xi,\omega) = G_i^*(\xi,\omega)s_i(\omega) = G_i(\xi,\omega)s_i^*(\omega) \tag{2}$$

where $f_i(\xi,\omega)$ is the reconstructed signal contributed by the strain $s_i(\omega)$, the superscript (*) denotes the complex conjugate of the variable. The reconstructed signals at any point in the structure from all the sensors can be expressed in the time domain as

$$\mathscr{F}(\xi, T-t) = \sum_{i=1}^{n} f_i(\xi, T-t) \tag{3}$$

where n is the number of sensors. T is the time duration of the T-R procedure determined by

$$T \geqslant t_\mathrm{d} + T_\mathrm{m} \tag{4}$$

where t_d is the estimated time duration of the impact force, t_m is time taken by the wave traveling from the source to the farthest sensor. Proper choice of T and n has been discussed in [32].

The T-R method is temporal and spatial focusing technique, the back-propagated wave-field converges toward the impact location, reaches the peak amplitude at the time of the impact and then diverges. The impact source

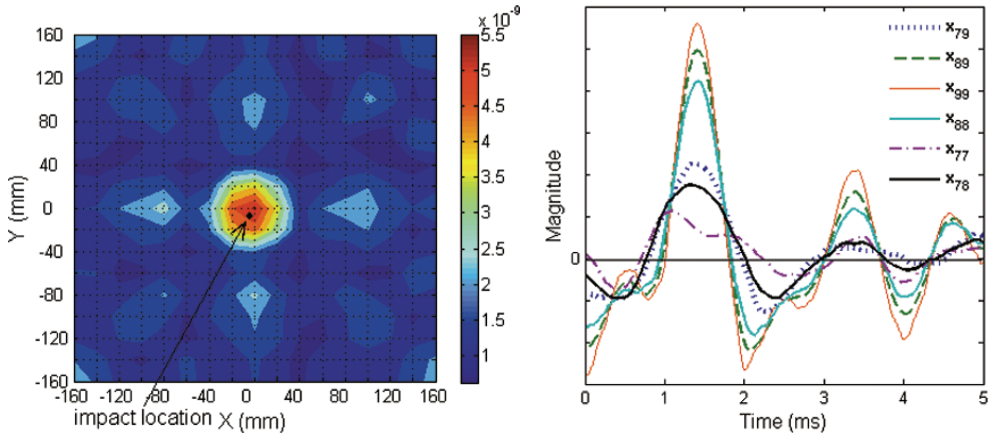

(a) (b)

Fig. 3. Results of T-R procedure for impact identifications (a) Contour plot of peak value of the reconstructed signals (b) Time history of reconstructed signals near impact location.

can be identified by selecting the maximum peak amplitude of the reconstructed signals for the entire time span among all locations in the plate. Figure 3 shows the results of T-R procedure of impact identifications in the plate impacted at the center of the plate. Figure 3(a) shows the contour plot of peak amplitudes of the reconstructed signals over the entire structure during T. The maximum peak amplitude of the reconstructed signals appears at the impact source location (spatial focusing). Figure 3(b) shows the time history of the time history of reconstructed signals near impact location. The impact force is a half-sinusoidal wave with time duration of 1 ms, and the impact location is $(-6, -4)$ mm. It can be shown in Fig. 3 that as the distance is closer to the impact source, the peak of the reconstructed force is higher and the maximum peak amplitude of the reconstructed force occurs at the impact source location at the initial impact time (temporal focusing).

2.2. Impact location detection

Based on T-R method, the maximum peak amplitude of reconstructed signals will refocus at the impact location and when at the impact is initiated. An adaptive two-step search algorithm is proposed to trace the impact location with high resolution. An initial search will be performed to roughly estimate the impact area by selecting the maximum peak amplitude among calibration locations. In T-R signal processing, the re-emitted signals converge at the impact source. Comparing the peak amplitude of the reconstructed signal at these calibration locations among calibration locations, $\mathbf{x}_{jk} \equiv (x_j, y_k)$, the maximum one is roughly estimated as the impact location. The peak amplitude of the reconstructed signals $P(\mathbf{x}_{jk})$ is defined as

$$P(\mathbf{x}_{jk}) = \underset{\text{at all times}}{\text{Max}} \left[\mathscr{F}(\mathbf{x}_{jk}, T - t)\right] \tag{5}$$

The first approximated impact location, denoted by $\hat{\mathbf{x}}$, is determined by

$$Q(\hat{\mathbf{x}}) = \text{Max}[P(\mathbf{x}_{jk})] \tag{6}$$

Figure 3(a) shows the contour plot of the peak amplitude of the reconstructed force at calibration locations over the plate. It is obvious to see that the trend of the contour line converges to the impact area. The maximum peak amplitude is at $\mathbf{x}_{99}(0, 0)$. Then a finer location search algorithm is proposed to determine the impact location more precisely in the impact area. The calibration locations will partition the plate into many small square areas. For example, in Fig. 3(a), the calibrated area is divided into 256 (16×16) square areas by 289 (17×17) calibration locations. The impact location is enclosed by a squared area whose vertexes are four calibration points. The area is chosen by the maximum peak amplitude at a calibration location and three other relatively high peak amplitudes

constituting the square area. In Fig. 3, impact location is enclosed the impact area whose vertexes are $\mathbf{x}_{88}(-20, -20)$, $\mathbf{x}_{89}(-20, 0)$, $\mathbf{x}_{98}(0, -20)$, and $\mathbf{x}_{99}(0, 0)$. Thus, the impact location can be further searched in this square area. The impact location is estimated in terms of the centroid of the peak amplitude of the reconstructed force at four calibration locations [13]. The centroid, $\hat{\hat{\mathbf{x}}}(x_e, y_e)$, is considered to be the finer impact location determined by

$$x_e = \frac{\sum_{j=1}^{4} x_j P(x_j, y_k)}{\sum_{k=1}^{4} P(x_j, y_k)}, \quad y_e = \frac{\sum_{k=1}^{4} y_k P(x_j, y_k)}{\sum_{k=1}^{4} P(x_j, y_k)} \tag{7}$$

where P is the peak amplitude of the reconstructed force at four calibration locations, which enclose the impact source. In Fig. 3(a), the approximate impact location $\hat{\mathbf{x}}$ is (0, 0), and the estimated impact location $\hat{\hat{\mathbf{x}}}$ is (−9.40, −9.19) mm.

The T-R method is a spatial energy focusing technique. $P(\mathbf{x}_{jk})$, the peak amplitude of the reconstructed signal is one of the parameters which could be used to search for impact location. The power of the peak amplitude, $W(\mathbf{x}_{jk})$ can be also used for impact location estimation.

In previous work [32], the time duration of T-R process T is about eight times that of the time duration of impact force t_f. The refocusing phenomenon is only in certain period T_1, which is shorter than T. Both the main packet and peak amplitude are in this period. Thus it is not necessary to check peak amplitude in the whole T, especially when T is much longer than the time duration of impact force. The time duration of the force could be estimated by analyzing the strain response in frequency domain. The maximum wave propagating time, t_m, can be readily estimated from experiments. In this work, $T_1 = 8$ ms and $t_\mathrm{f} = 1$ ms, $t_\mathrm{m} = 1$ ms, set $T_1 = 3$ ms. Selecting the peak amplitude in T_1 will reduce the computation time and improve the stability of the impact location detection especially the spacing of calibration location is larger and the signals are contaminated with noise. It will be discussed in detail in Section 3.

2.3. Force reconstruction

The computation of the T-R method used in this work is a simple operation, and only transfer function and strain response are used in T-R process, thus only partial information of the force, such as the time history of the shape, could be reconstructed by incomplete information. Based on transfer functions, the shape of the loading history and the impact location are obtained in impact location estimation simultaneously. Once the impact location and the shape of the impact force are obtained by the T-R method, the magnitude of the force can be calculated by comparing the response signals measured by the sensors with the response signals predicted by shape of the force and the transfer functions. The predicted response signals are computed by

$$\mathscr{S}_i(\omega) = \mathscr{F}(\hat{\hat{\mathbf{x}}}, \omega) G_i(\hat{\hat{\mathbf{x}}}, \omega) \tag{8}$$

This computation is a forward process. The first estimated scaling factor $\hat{k}$ is calculated as

$$\hat{k} = \frac{1}{n} \sum_{i=1}^{n} \left[\frac{\sum_{t=0}^{T} |s_i(t)|}{\sum_{t=0}^{T} |\mathscr{S}_i(t)|} \right] \tag{9}$$

where $s_i(t)$ is the response signal measured by sensors and, $\mathscr{S}_i(t)$ is the predicted response signal in time domain. Then a finer magnitude search algorithm based on a least-squares method is proposed to determine the magnitude of the force more accurately. It is written as

$$E(k) = \frac{1}{n} \sum_{i=1}^{n} \left[\sum_{t=0}^{T} |s_i(t)|^2 - k^2 \sum_{t=0}^{T} |\mathscr{S}_i(t)|^2 \right] \tag{10}$$

Table 1
Mean error and standard deviation in impact location detection

Impact events	△ = 20 mm		△ = 40 mm	
	$P(\mathbf{x}_{jk})$	$W(\mathbf{x}_{jk})$	$P(\mathbf{x}_{jk})$	$W(\mathbf{x}_{jk})$
#1	1.56	3.10	6.31	1.75
#2	6.73	6.26	11.88	9.31
#3	4.84	3.53	5.81	3.16
#4	7.13	6.21	13.31	7.18
#5	6.20	5.20	11.24	1.98
#6	8.56	7.24	9.54	4.65
#7	2.69	1.67	9.15	1.99
#8	7.66	6.42	16.44	8.04
#9	12.11	3.48	18.17	6.96
Mean error	6.39	4.79	11.32	5.00
Standard deviation	2.96	1.79	3.95	2.76

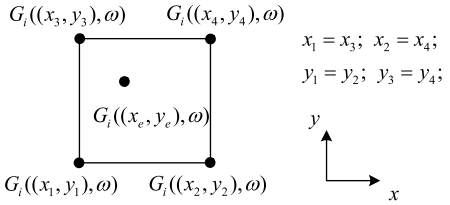

Fig. 4. Approximation of transfer function at estimated impact location.

The minimum amplitude of $E(k)$ is calculated as $E(\hat{\hat{k}})$ in the range $[0.5\hat{k}, 1.5\hat{k}]$.

In general, the estimated impact location is not at the calibration locations. To approximate transfer functions at estimated impact location using those at neighboring calibration locations [13] in reconstructing impact force, the transfer functions at estimated location can be linearly interpolated from transfer functions at four calibration locations given below and shown in Fig. 4.

$$G_i(\hat{\hat{\mathbf{x}}}, \omega) = \sum_{j=1}^{4} \eta_j G_i(\mathbf{x}_{jk}, \omega) \tag{11}$$

where $\eta_1 = (1-\alpha)(1-\beta)$, $\eta_2 = \alpha(1-\beta)$, $\eta_3 = (1-\alpha)\beta$, $\eta_4 = \alpha\beta$, $\alpha = (x_e - x_1)/(x_2 - x_1)$, $\beta = (y_e - y_2)/(y_3 - y_2)$. As shown in Fig. 3, $G_i(\hat{\hat{\mathbf{x}}}, \omega)$ can be approximated by $G_i(\mathbf{x}_{88}, \omega)$, $G_i(\mathbf{x}_{89}, \omega)$, $G_i(\mathbf{x}_{98}, \omega)$, and $G_i(\mathbf{x}_{99}, \omega)$.

It is noted that the approximated transfer functions can be used to reconstruct the shape of the force, but not for detecting impact location. Based on the refocusing property of T-R method, the impact location determined by selecting the maximum peak amplitude of reconstructed signals in time domain, however, the peak amplitude of the signals reconstructed by approximated transfer functions can not be larger than the maximum peak amplitude among the four calibration locations around it. It can be illustrated by

$$P(\hat{\hat{\mathbf{x}}}) = \operatorname{Max}_{t}[\mathscr{F}(\hat{\hat{\mathbf{x}}}, T-t)] < \operatorname{Max}_{j=1,2,3,4}[P(\mathbf{x}_{jk})] \sum_{j=1}^{4} \eta_j = \operatorname{Max}_{j=1,2,3,4}[P(\mathbf{x}_{jk})] \tag{12}$$

The shape of the force reconstructed by the T-R method is not exact as that of the original one. In this procedure the opposite sign of the reconstructed impact force is intentionally removed because the impact force acts in a single direction towards the plate. In practice, the main impact energy is in the main wave packet. To determine the scaling factor of the impact more seriously, only the main packet wave is selected as the shape of the force.

3. Numerical results and discussion

3.1. The spacing resolution of the calibration locations

Although it is impractical to calibrate the plate at every location, more precise impact source can be obtained if the calibration locations are denser. However, the number of calibration locations and time spent in computation for force identification will increase rapidly with the increase of the density of the calibration locations. For example, the number of calibration locations will increase from 81 (9×9) to 249 (17×17) when the spacing of calibration location reduces by half from 40 mm to 20 mm. Thus a tradeoff needs to be made between the resolution of the

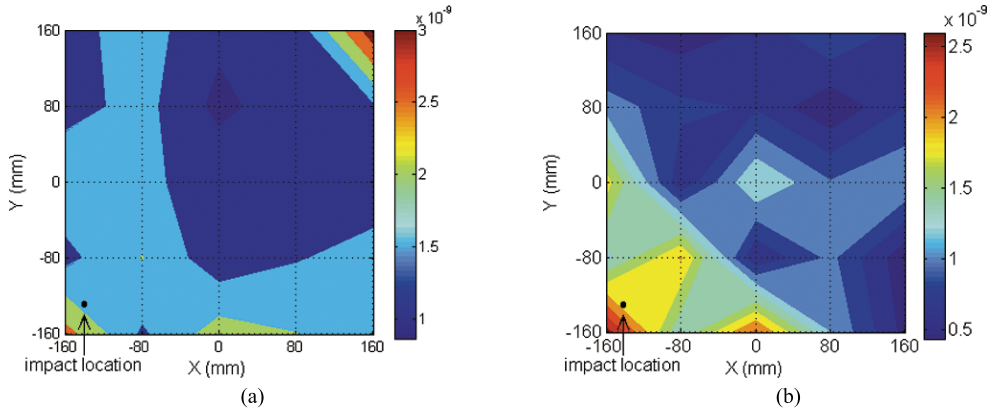

Fig. 5. Initial search results of impact #2 (a) Selecting the peak value during time period T (b) Selecting the peak value during time period T_1.

transfer function and time spent in computation. The spacing of the calibration locations is chosen from 20 mm to 80 mm by 20 mm in spacing increment.

The impact locations are searched in two steps as discussed in previous Section. The small impact square area enclosing the impact location is detected first followed by a finer search. If the square region covering the impact is not located correctly, the impact location can not be traced accurately. In T-R refocusing, the peak amplitude of the reconstructed signal decreases away from the impact location. In selecting the appropriate calibration location spacing procedure, the impact location is always chosen at the center of each square area. Due to symmetric geometry of the plate, only a quarter of the plate is needed to be calibrated. Without loss of generosity, the plate is also considered to be impacted in this region.

The critical calibration location was investigated on plate with 1 mm thickness first. All the impact locations can be accurately detected in the square region when the spacings of the calibration are 20 and 40 mm, while only one is detected correctly when the spacing is 60 mm. It is noted that all the impact loading time-histories in this study are identical, a half-sinusoidal wave with the 1 ms time duration and 40 N peak force. The impact area is also detected correctly when the time duration of the force is 100 μs, i.e., higher frequency, and the spacing of the calibration location remains 40 mm. For this plate with 1 mm thickness, the result is insensitive to the frequency of the impact force.

The accuracy of impact location detection is directly related to the calibration location spacing of the transfer functions. To investigate the effect of spacing of calibration locations and the relative position between impact location and calibration location for impact source identification based on T-R method, nine impact locations in one quarter of 1 mm thickness plate are detected under two calibration spacing densities, 20 mm and 40 mm. The peak amplitude $P(\mathbf{x}_{jk})$ through T is selected as the characteristic parameter to trace the impact location first. The results are shown in Table 1. All the impact square areas covering the impact locations are detected correctly. The average error is about one quarter of the length of the impact square area when $\triangle = 40$ mm. The average error and the standard deviation increase with the increase of the spacing of the calibration location. The same conclusion as shown in Table 1 is made when the power of the peak amplitude $W(\mathbf{x}_{jk})$ through the period T. The effect of the spacing of the calibration location decreases by selecting $W(\mathbf{x}_{jk})$. Comparing the average and the standard deviation, the results are improved when the signal power $W(\mathbf{x}_{jk})$ is used. It is noted that the unit in all tables are mm.

The capability of finding the impact location relies on the shortest distance between impact location and the calibration location. In previous discussion, the impact area can not be detected correctly when $\triangle = 60$ mm when the impact is hit at the center of the small square. However, only #5 and #7 are not detected correctly in the initial search step when $\triangle = 60$ mm. Some of the impact locations still can be detected when $\triangle = 80$ mm, such as #1, #3, #5, #7 and #9 due to the shortest distance between these locations and the calibration locations being still sufficiently small. It means that only the center location of in each square area covered by four calibration locations is needed to be checked in determining the calibration spacing. The maximum amplitude of the shortest distance between impact locations and the calibration location is $20\sqrt{2}$ mm when $\triangle = 40$ mm. It may be summarized from the plate studied

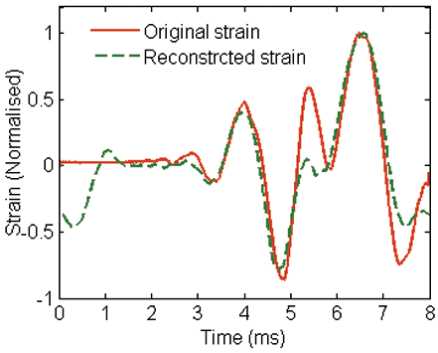

Fig. 6. Shapes of strain by sensor 3 in impact #3 compared with the original strain response.

that when the distance between the impact location and the calibration location is shorter than 20 $\sqrt{2}$ mm, the impact location can be accurately located.

Results can be improved by selecting the peak amplitude through T_1. If $\triangle$ = 80 mm, #2 is detected correctly in the initial search step and #4 and #8 are detected in the neighboring square area by selecting the peak amplitude through T_1. The results of the initial search step for #2 are shown in Fig. 5. The result of the initial impact location detection will be improved if the peak amplitude is limited in the "refocusing" period T_1. In the flowing discussion about the loading time-history reconstruction and the effect of the noise, the spacing of calibration location is set as $\triangle$ = 40 mm and the power of the peak amplitude $W(\mathbf{x}_{jk})$ through T_1 is chosen in impact location estimation for 1 mm thickness plate.

The spacing resolution of calibration locations plays a critical role in the accuracy of the impact source identification. To investigate the relationship between critical spacing and the thickness of the plate, aluminum flat plates with the in-plane dimensions 420 mm×420 mm with two thicknesses, 2 mm and 4 mm, were also built in FEM model and impact location detections on these two plates were studied. It is noted that all impact locations are set at the center of the impact area as that of 1 mm thickness plate. For 2 mm thickness plate, all impact locations can be detected at right impact area when $\triangle$ = 40 mm, most impact locations are detected correctly except three impact locations were detected at neighbor impact area when $\triangle$ = 60 mm, and only one impact location was detected at right impact area when $\triangle$ = 80 mm. The results of the 4 mm thickness plate were similar as that of 2 mm, but more impact locations can be detected when $\triangle$ = 60 mm and $\triangle$ = 80 mm. The results of impact locations detection on 2 mm and 4 mm plates are better than that of 1 mm plate. Wider spacing of the calibration locations can be selected for impact location detection with the increase of the plate thickness. It is not necessary compute the relationship between the critical spacing resolution of the calibration locations and the thickness of the plate quantitatively here, because the true structures are more complex, not only flat plates. To quantify the effect of plate thickness on impact location detection by T-R method with discrete transfer functions, more theoretical and experiment studies are needed. The conclusion about the spacing of calibration locations and the thickness of plate can be used to guide the selection of the calibration spacing in impact identification in practice. In summary, the impact location detection was related to the spacing resolution of the calibration locations; the selection of parameters in T-R process and in the following searching method was suggested.

3.2. Impact force time-history reconstruction

After the transfer functions $G_i(\hat{\mathbf{x}}, \omega)$ between the estimated impact location and the sensors are approximated, the shape of the force can be reconstructed by T-R procedure and the scaling factor can be determined by the method developed from previous section. It is noted that only the main pulse packet of the reconstructed force is considered. Figure 6 shows the strains measured by sensor and the one reconstructed by transfer functions. The reconstructed force in #3, #6 and #7 are shown in Fig. 7. The peak force of the reconstructed impact load history in #3, #6 and #7 are 42.3 N, 47.7 N, and 40.3 N respectively. If the opposite sign portion of the reconstructed signals is not neglected in determining the scaling factor, the peak force of reconstructed impact load history in #3, #6 and #7 are 32.8 N, 24.5 N, and 24.8 N respectively. The results show that it is reasonable to select the main packet wave of the

Table 2
Mean error and standard deviation in impact location detection with noises contained in signals

Impact events ($\triangle$ = 40 mm, $W(\mathbf{x}_{jk})$)	Uniform distributed noise						Gaussian noise
	In strain		In transfer functions		In both		In both
	20 dB	10 dB	20 dB	10 dB	20 dB	10 dB	10 dB
#1	1.59	0.89	2.40	0.48	1.59	2.22	1.63
#2	9.97	9.21	9.90	9.35	10.18	11.33	15.95
#3	3.45	2.76	4.23	5.38	3.37	6.65	6.60
#4	7.52	9.05	8.01	12.12	8.31	14.22	6.64
#5	2.86	1.93	0.73	1.38	2.35	4.09	2.34
#6	4.56	5.34	4.79	4.78	5.57	4.88	6.43
#7	2.95	3.10	3.09	5.00	3.28	11.05	6.40
#8	8.90	9.11	9.23	12.21	9.82	12.47	9.03
#9	9.54	10.04	8.38	9.42	9.74	13.26	11.93
Mean error	5.70	5.71	5.64	6.68	6.02	8.91	7.44
Standard deviation	3.08	3.44	3.13	4.08	3.31	4.21	4.19

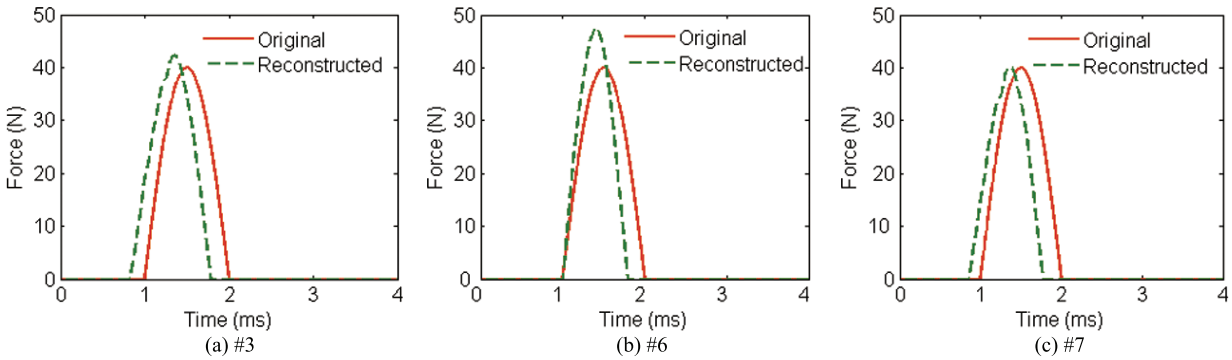

Fig. 7. Impact force time-history reconstructions.

reconstructed signals in T-R process as the shape of the force for impact loading history reconstruction. For the error in impact location detection and transfer function approximation, there are some deviations from the true impact loading time-history in strain and force reconstructions. Similar results are obtained from the remaining of the six locations. The main shapes of the force are reconstructed successfully. For the force scaling factor determination is based on the energy conservation, the peak force is overestimated when the time duration of the reconstructed force is shorter than that of the true impact force, such as Figs 7(a) and (b), and vice versa. The results of the force reconstruction may originate from the error in impact location detection and the relative position of the impact location in the plate.

3.3. The effect of noise

In practice, the signals measured by the sensors are distorted by noise. The noise may be caused by the surrounding environment, sensors, data acquisition, and other unknown sources. The noise often leads to inaccurate and unstable results, especially for inverse problems [4]. To investigate the reliability and stability of the T-R method for impact source identification, noise is added into strain response and/or transfer functions. Two types of the noise, uniform distributed or Gaussian, are used to simulate the noise state in practice. In this work, the noise signals are generated by MATLAB code, and then added into signals. The intensity of the noise is considered to determine the noise tolerance of T-R method under various conditions.

In [32], the T-R method is robust against uniform distributed noise in force reconstruction. In this work, the main objective focuses on the effect of noise in both impact location estimation and the force reconstruction by the approximated transfer functions, rather than just in impact force reconstruction. The signal noise ratio (SNR) is defined in [32]. The uniform distributed noise is studied followed by the Gaussian noise. First, uniform distributed noise is only added into the response strain. Table 2 shows the results of the impact location estimation when two

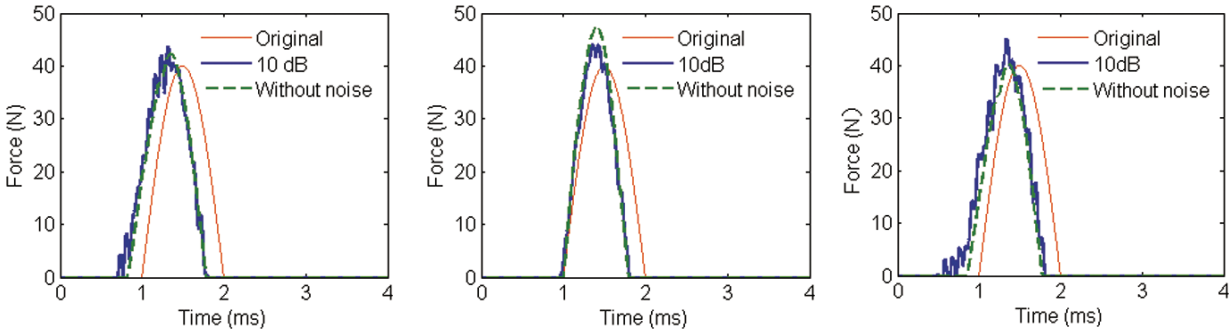

Fig. 8. Impact force time-history reconstructions with uniform distribution noise.

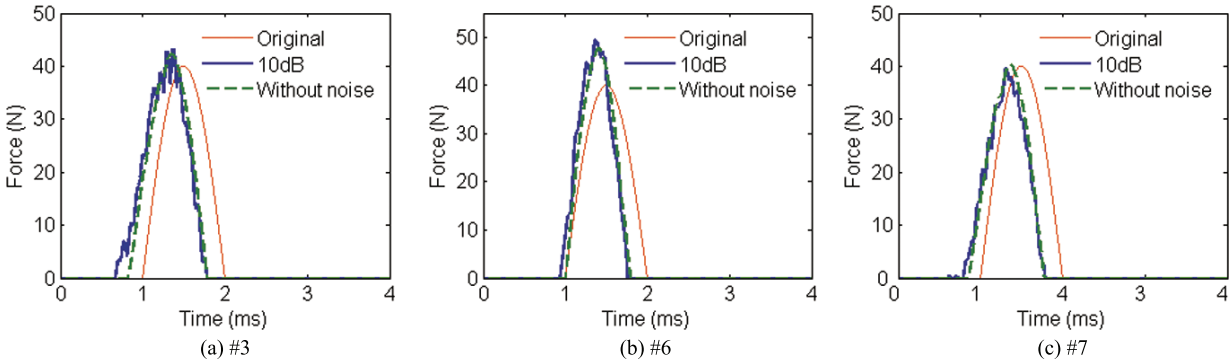

Fig. 9. Impact force time-history reconstructions with Gauss distribution noise.

types of noise are added into the signals, SNR = 20 dB, 10 dB. Comparing the results of the first and second row in Table 2 with the results in Table 1, uniform distributed noise contaminated only in response strain affects the accuracy of impact location detection slightly. Both the average error and the standard deviation increase slightly when the noise level increases from SNR = 20 dB to 10 dB.

The third and fourth row in Table 2 show the results of the impact location estimation when the uniform distributed noises are contaminated into the transfer functions, SNR = 20 dB, 10 dB respectively. The effect of the noise in transfer function shows a very similar trend as that of noise in strain response; the average error and the standard deviation caused in transfer function are slightly larger than that of the noise contaminated in strain. They also increase more rapidly with the increase of noise amplitude. Thus for impact location detection, the results are more sensitive to the noise in transfer function than that in strain. It is in agreement with the conclusion in force reconstruction in previous work.

In practice, both the transfer function and the strain may be contaminated with noise. The results of the impact location detection when noise in both transfer functions and strains are shown in the fifth and sixth rows in Table 2. The results are similar but are less accurate than those where the noise is contained either in transfer functions or in strains. The average error is less than a quarter of the spacing of transfer function, 40 mm. The impact locations can be detected accurately even both transfer function and strains are contained with 10 dB noise.

The impact loading time-history at different impact locations are also well reconstructed by approximated transfer functions when 10 dB noises are both in transfer functions and strains. Figure 8 shows the reconstruction of the forces at #3, #6, and #7. Forces are reconstructed successfully though 10 dB noises are in transfer functions and response strains though there are some errors in impact location detection and transfer function approximation.

Gaussian noise is also considered to investigate the stability of T-R method for impact source identification. The last row in Table 2 shows the results of the impact location detection when 10 dB Gaussian noise contained both in transfer functions and strain response. The average error and standard deviation are close to that of 10 dB uniform distributed noise. Figure 9 show the result of force reconstruction at #3, #6 and #7 when transfer functions and

strains are added 10 dB Gaussian noise. Forces can also be reconstructed accurately as well as the impact location detection under 10 dB Gaussian noise. The conclusion of Gaussian noise is similar to that of uniform distributed noise. The T-R method is robust against with noise for its super stability and reliability.

4. Conclusions

An impact source identification method based on synthetic T-R concept has been examined to trace the impact location and reconstruct the impact loading time-history. The issue of calibration spacing in characterizing the plate using transfer functions in impact identification is investigated in detail. A two-step impact location detection method is developed. The scaling factor of the force is computed based on conservation of signal energy after the impact location and the shape of the force are obtained. Other issues including parameter selection, transfer function approximation and effect of noise are discussed. The conclusions may be drawn as follows.

1) The resolution of the impact area detection depends on the distance from the impact location to the nearest calibration location. The permissible calibration spacing increases with the increase of plate thickness. The average error and its standard deviation of the impact location detection increase with the increase of the spacing of calibration locations.
2) The main shape of the impact loading time-history can be well reconstructed at different impact locations. The impact loading time-history reconstruction depends on the location impacted in the plate, the accuracy of impact location detection and the transfer functions approximation.
3) The effects of Gaussian and uniform distributed noise on impact location detection and the force reconstruction are investigated. The results show that the T-R method is robust against noise.

In summary, this work provides the guidance of T-R method for impact source identification. The simulation study can be utilized to guide the selection of spacing of the calibrated transfer function in experiments. The T-R method is robust against noise and the ill-conditioned inverse problem has been overcome. The T-R method is suited to monitoring the impact events in complex structures near real-time.

Acknowledgments

Mr. Chen is appreciated by the support from National Natural Science Foundation of China (No.10932008) and the 111 project (No.B07050). This paper is partially supported by the AFOSR Grant No. FA9550-09-C-0140 through Acellent Technologies Inc. on STTR Phase I effort.

References

[1] S.R. Reid and G. Zhou, Impact behaviour of fibre-reinforced composite materials and structures, CRC Press, Boca Raton, Woodhead Publishing Limited, Cambridge, England, 2000.
[2] D.E. Bray and D. McBride, Nondestructive testing techniques, John Wiley & Sons, Inc., New York, 1992.
[3] J. Hadamard, Lectures on the Cauchy problem in linear partial differential equations, Yale University Press, New Haven, 1923.
[4] H. Inoue, J.J. Harrigan and S.R. Reid, Review of inverse analysis for indirect measurement of impact force, *Applied Mechanics Reviews* **54** (2001), 503–524.
[5] J.H. Dibiase, H.F. Silverman and M.S. Brandstein, in: *Microphone arrays signal processing techniques and applications*, Chapter 8, M. Brandstein and D. Ward, eds, Springer, New York, 2001, pp. 157–180.
[6] R. Seydel and F.K. Chang, Impact identification of stiffened composite panels: I system development, *Smart Materials & Structures* **10** (2001), 354–369.
[7] Y.C. Yang and K.S. Han, Damage monitoring and impact detection using optical fiber vibration sensors, *Smart Materials & Structures* **11** (2003), 337–345.
[8] M. Meo, G. Zumpano, M. Piggott and G. Marengo, Impact identification on a sandwich plate from wave propagation response, *Composite Structures* **71** (2005), 302–306.
[9] L. Gaul and S. Hurlebaus, Identification of the impact location on a plate using wavelets, *Mechanical Systems and Signal Processing* **12** (1998), 783–795.
[10] Y. Ding, R.L. Reuben and J.A. Steel, A new method for waveform analysis for estimating AE wave arrival times using wavelet decomposition, *NDT&E International* **37** (2004), 279–290.

[11] T. Kundu, S. Das, S.A. Martin and K.V. Jata, Locating point of impact in anisotropic fiber reinforced composite plates, *Ultrasonics* **48** (2008), 193–201.
[12] H. Fukunaga and N. Hu, Health monitoring of composite structures based on impact force identification, in: *Proceedings of the 2nd European Workshop on Structural Health Monitoring* Munich, Germany, (2004), 415–422.
[13] J. Park and F.K. Chang, System identification method for monitoring impact events, in: *Smart Sensor Technology and Measurement System*, *Proceedings of the SPIE* San Diego, CA, (2005), 189–200.
[14] J. Park, S. Hu and F.K. Chang, Monitoring impact events using a system-identification method, *AIAA Journal* **47** (2009), 2011–2021.
[15] J. Markmiller and F.K. Chang, Sensor network optimization for a passive sensing impact detection technique, *Structural Health Monitoring* **9** (2010), 25–39.
[16] J. Haywood, P.T. Coverley, W.J. Staszewski and K. Worden, An automatic impact monitor for a composite panel employing smart sensor technology, *Smart Materials & Structures* **14** (2005), 265–271.
[17] L. Gaul and S. Hurlebaus, Determination of the impact force on a plate by piezoelectric film sensors, *Archive of Applied Mechanics* **69** (1999), 691–701.
[18] E. Wu, T.D. Tai and C.S. Yen, Two methods for determining impact-force history on elastic plates, *Experimental Mechanics* **35** (1995), 11–18.
[19] C. Chang and C.T. Sun, Determining transverse impact force on a composite laminate by signal deconvolution, *Experimental Mechanics* **29** (1989), 414–419.
[20] E. Jacquelin, A. Bennani and P. Hamelin, Force reconstruction: Analysis and regularization of a deconvolution problem, *Journal of Sound and Vibration* **265** (2003), 81–107.
[21] A.D. Steltzner and D.C. Kammer, Input force estimation using an inverse structural filter, in: *17th International Modal Analysis Conference* Kissimmee, FL, (1999), 954–960.
[22] K. Chandrashekhara, O.A. Chukwujekwu and Y.P. Jiang, Estimation of contact force on composite plates using impact-induced strain and neural networks, *Composites*, *Part B: Engineering* **29** (1998), 4363–4370.
[23] M. Fink, Time reversal of ultrasonic fields-Part I: Basic principles, *Ultrasonics, Ferroelectrics, and Frequency Control* **39** (1992), 555–566.
[24] M. Fink, Time-reversal acoustics in complex environments, *Geophysics* **71** (2006), SI151–164.
[25] H. Kawakatsu and J.P. Montagner, Time-reversal seismic-source imaging and moment-tensor inversion, *Geophysical Journal International* **175** (2008), 686–688.
[26] H. Sohn, H.W. Park, K.H. Law, and C.R. Farrar, Damage detection in composite plates by using an enhanced time reversal method, *Journal of Aerospace Engineering* **20** (2007), 141–151.
[27] C.H. Wang, J.T. Rose and F.K. Chang, A synthetic time-reversal imaging method for structural health monitoring, *Smart Materials & Structures* **13** (2004), 413–423.
[28] B. Xu and V. Giurgiutiu, Single mode tuning effects on lamb wave time reversal with piezoelectric wafer active sensors for structural health monitoring, *Journal of Nondestructive Evaluation* **26** (2007), 123–134.
[29] H.W. Park, H. Sohn, K.H. Law and C.R. Farrar, Time reversal active sensing for health monitoring of a composite plate, *Journal of Sound and Vibration* **302** (2007), 50–66.
[30] F. Ciampa and M. Meo, Impact detection in anisotropic materials using a time reversal approach, *Structural Health Monitoring* **0** (2011), 1–7.
[31] L. Qiu, S.F. Yuan, X. Zhang and Y. Wang, A time reversal focusing based impact imaging method and its evaluation on complex composite structures, *Smart Materials and Structures* **20** (2011), 105014.
[32] C. Chen and F.G. Yuan, Impact source identification in finite isotropic plates using time-reversal method: Theoretical study, *Smart Materials and Structures* **19** (2010), 10528.